

Next-Generation Wound Care: Aptamer-Conjugated Polydiacetylene/Polyurethane Nanofibrous Biosensors for Selective In Situ Colorimetric Detection of *Pseudomonas*

Sarah Currie, Alan Jesus Cortes de la Torre, Ayush Kumar, Sarvesh Logsetty, and Song Liu*

Biosensors for wound dressings can enable point-of-care monitoring of wound bed health by exhibiting a color change visible to the naked eye, to alert healthcare providers of the presence of pathogenic bacteria. Here, a polydiacetylene-based electrospun nanofibrous wound dressing for the detection of *Pseudomonas aeruginosa* is reported. Using conventional blend electrospinning, two diacetylene monomers—10,12-pentacosadiynoic acid (PCDA) and 10,12-tricosadiynoic acid (TCDA)—are separately electrospun alongside polyurethane as a supporting matrix polymer. The differences in side-chain length impact the sensitivity of the nanofibers in detecting *P. aeruginosa*. Furthermore, two DNA aptamers are conjugated to the polydiacetylenes to achieve targeted detection of *P. aeruginosa*. The aptamer-modified dressings show improved sensitivity of detection toward eight strains of *P. aeruginosa* compared to the unmodified membranes. Furthermore, the aptamer-modified membranes do not respond to non-target bacteria methicillin-resistant *Staphylococcus aureus* (MRSA), *Staphylococcus aureus*, and *Escherichia coli* within 3 h of direct contact. Reducing the chain-length of the diacetylene monomer by substituting PCDA with TCDA boosts the colorimetric response by a factor of >2x compared to the aptamer-modified PCDA membranes, at the cost of reduced specificity. The aptamer-conjugated polydiacetylene membranes show promise for application in point-of-care wound dressings for improved specificity of detection of bacterial infections.

in chronic and burn wounds.^[1–4] *P. aeruginosa* infection in burn wound patients results in up to 80% mortality.^[5,6] Furthermore, the emergence of antibiotic-resistant strains of bacteria due to antibiotic use is a major issue facing wound care. Multidrug-resistant strains of *P. aeruginosa* have become increasingly prevalent in clinical settings, displaying resistance to a wide range of antibiotic classes including beta-lactams, aminoglycosides and fluoroquinolones.^[7] Early diagnosis of bacterial infection is crucial for curbing the emergence of antibiotic-resistant strains. This is particularly true for infections caused by highly adaptable pathogens like *P. aeruginosa*. Prompt and accurate diagnosis empowers healthcare providers to implement effective treatment strategies with appropriate antibiotics. This targeted approach minimizes the indiscriminate use of antibiotics, thereby significantly reducing the selective pressure that drives the development of resistance.^[8] The development of a rapid point-of-care test for *P. aeruginosa* wound infection would be a valuable tool for healthcare providers. Such a test would enable timely and effective treatment, ultimately

1. Introduction

Pseudomonas aeruginosa is a major opportunistic wound pathogen, and is one of the most commonly isolated bacteria

improving patient outcomes and reducing the risk of evolved antibiotic resistance.

Diagnostic wound dressings can be designed to meet these needs for rapid and accurate in situ monitoring of wound bed

S. Currie, S. Liu
Department of Biosystems Engineering
Faculty of Agricultural and Food Sciences
University of Manitoba
Winnipeg, Manitoba Canada
E-mail: song.liu@umanitoba.ca

The ORCID identification number(s) for the author(s) of this article can be found under <https://doi.org/10.1002/adfm.202403440>

© 2024 The Author(s). Advanced Functional Materials published by Wiley-VCH GmbH. This is an open access article under the terms of the [Creative Commons Attribution-NonCommercial-NoDerivs](#) License, which permits use and distribution in any medium, provided the original work is properly cited, the use is non-commercial and no modifications or adaptations are made.

DOI: 10.1002/adfm.202403440

A. J. Cortes de la Torre
Research Laboratory on Optimal Design
Devices and Advanced Materials – OPTIMA
Department of Mathematics and Physics
ITESO
Tlaquepaque, Jalisco Mexico

A. Kumar
Department of Microbiology
Faculty of Science
University of Manitoba
Winnipeg, Manitoba Canada

S. Logsetty
Departments of Surgery
Psychiatry
and Children's health Rady Faculty of Health Sciences
University of Manitoba
Winnipeg, Manitoba Canada

health in clinical settings. Current advancements have focused on developing sensors that detect various stimuli associated with wound infection. These include bacterial toxins, enzymes, pigments (such as *P. aeruginosa*'s pyocyanin), metabolites (urate), lipopolysaccharide, and host immune response markers such as neutrophils enzymes (elastase and cathepsin G) and elevated wound pH.^[9–19] This progress has undoubtedly improved wound management. However, a significant gap exists in our ability to identify specific bacterial species within infected wounds at the point of care. Common detection signals such as pH may not always be a reliable indicator of infection, since pH levels can fluctuate throughout wound healing in response to tissue damage, inflammation, and the presence of medications. Herein lies the impetus for our research. We aim to bridge this gap by developing a novel diagnostic approach that enables the in situ pinpointing of *P. aeruginosa* infection within the wound environment. By identifying the bacteria responsible for the infection, we can tailor treatment strategies to ultimately promote faster healing and improved patient outcomes. Furthermore, the sensitivity of detection remains a barrier to the clinical implementation of such dressings. Ideally, diagnostic dressings for wound infections should be capable of detecting bacterial concentrations at the critical threshold defining the transition from wound “colonization” to wound “infection”: $5 \times 10^4 - 4.6 \times 10^5$ CFU/cm².^[20–22] Our major advancement in these two key areas is based on two unique strategies to tailor the dressing's specificity and sensitivity. First, two aptamers were carefully selected to bind *P. aeruginosa* to achieve enhanced specificity of detection. Second, polydiacetylene was used as the colorimetric element of the biosensor, with a controlled selection of the diacetylene composition to boost the sensitivity of detection.

Polydiacetylenes are polymers with a conjugated backbone formed of alternating double and triple bonds resulting in a characteristic deep blue absorbance at 640 nm, formed from 1,4-addition reaction between diacetylene monomers by UV polymerization.^[18,23–30] A variety of stimuli (such as heat, pressure and organic molecules) can induce a conformational change in the backbone of the polymer resulting in a color change from blue to red and a shift in characteristic absorbance from 640 to 540 nm.^[26] Polydiacetylenes have been used to detect bacteria through the interaction of bacterial excretions with the side chains of polydiacetylene and typically are implemented as a detection element in vesicles or liposomes. In several studies, polydiacetylenes have been successfully incorporated into electrospun nanofibers for the detection of volatile organic compounds^[25] or *E. coli*.^[18] Furthermore, the pendant side chains of polydiacetylenes can be modified through the conjugation of targeting molecules such as peptides, glycolipids, aptamers, antibodies or small molecules to the pendant side chains to achieve color changes in response to a desired stimulus.^[23–26,29–31] Aptamers are short single-stranded sequences of DNA or RNA capable of selectively binding targets such as small molecules, proteins or whole cells; and are particularly appealing as targeting

elements due to their high specificity and binding affinity for the target substrate.^[32]

In this study, we present aptamer-conjugated polydiacetylene nanofibers capable of responding with high specificity and sensitivity to a chosen specific strain of *P. aeruginosa*. Two different diacetylene monomers, 10,12-pentacosadiynoic acid (PCDA), and 10,12-tricosadiynoic acid (TCDA), were combined with polyurethane (PU) as a supporting matrix to create nanofibers with controlled sensitivity. Furthermore, aptamers targeting *P. aeruginosa* were conjugated to the polydiacetylenes to improve the sensitivity and specificity of the fibers. Two aptamers were chosen for conjugation to the polydiacetylene membranes – aptamer F₂₃^[33] and St21Lp17.^[34] The aptamer-modified biosensing nanofibers demonstrated higher sensitivity toward eight *P. aeruginosa* strains compared to the unmodified membranes (ATCC 27853, PA01, PA0200, PA0238, PA0325, PA0386, PA01172, and 73104). Furthermore, boosted sensitivity of detection was achieved by replacing the PCDA monomer in the membrane with a shorter chain-length monomer, TCDA. The aptamer-modified membranes did not respond non-specifically to non-target bacteria lawns of *Escherichia coli* or methicillin-resistant *Staphylococcus aureus* (MRSA), which confirms the feasibility of aptamer-based targeting for bacteria detection. The strategy of aptamer-modification of polydiacetylene nanofibers for detection of wound infections shows promise for the development of a point-of-care in situ wound biosensor with improved specificity of detection.

2. Results and Discussion

2.1. Characterization

Polydiacetylene nanofibers are commonly fabricated by blend electrospinning diacetylene monomers with a supporting matrix polymer such as poly(ethylene oxide), PU, poly(methyl methacrylate) or polystyrene.^[18] Self-assembly of the diacetylene monomers occurs during electrospinning, which facilitates UV-polymerization of the monomers after electrospinning via a 1,4-addition reaction. In this study, PU was selected as a matrix polymer to facilitate the electrospinning of two different diacetylene monomers (PCDA or TCDA). Nanofiber morphology was assessed using scanning electron microscopy (SEM) (**Figure 1**). The fibers had smooth surface morphology and continuous fiber structure without evidence of beading. The average fiber diameters of the as-spun unmodified membranes were 120 ± 53 nm and 117 ± 39 nm for P and T respectively. Small fiber diameter is desirable for application as a diagnostic biosensor, since higher specific surface area increases the probability for interactions between the bacteria and fiber surface. It is well recognized that the high surface-to-volume ratio of nanofibers is key for biosensor sensitivity, by giving increased surface area for interaction with analytes as well as more area for conjugation of targeting moieties.^[36,37] After the wet post-spinning modification of the N-hydroxysuccinimide (NHS)-activated PCDA groups with aptamers F₂₃ or St21Lp17, the aptamer-modified membranes had larger fiber diameter compared to the as-spun membranes, ranging from 164–225 nm. Evidently, the wet-modification process for aptamer conjugation resulted in swelling of the PU fiber matrix and larger fiber diameter.

S. Liu
Biomedical Engineering
Faculty of Engineering
University of Manitoba
Winnipeg, Manitoba Canada

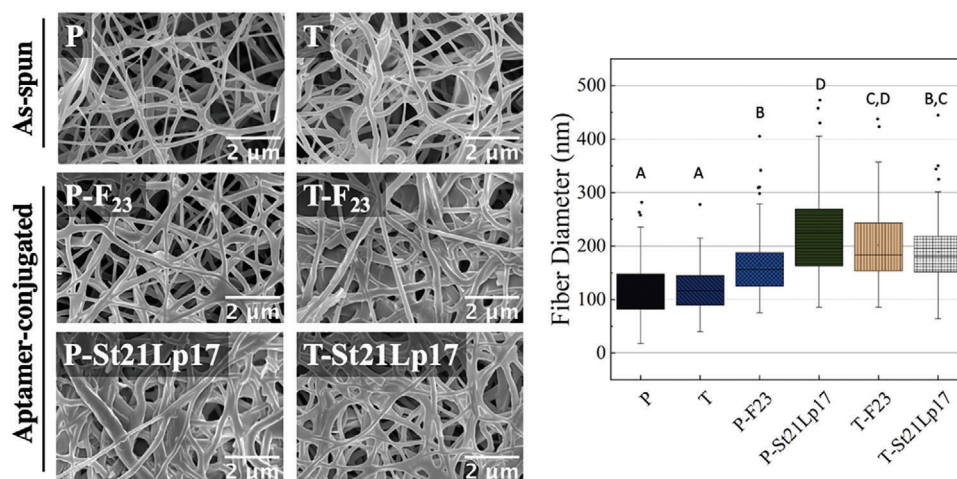


Figure 1. SEM images of electrospun nanofibers before and after aptamer conjugation. Different letters (A, B, C, D) indicate significant differences by ANOVA with Tukey correction, $n = 100$ ($p < 0.05$).

The electrospun membranes were analyzed with attenuated total reflectance Fourier transform infrared spectroscopy (ATR-FTIR) to confirm the successful incorporation of each of the constituent components (Figure 2). First, the monomer and polymer starting materials were characterized with ATR-FTIR prior to electrospinning to identify the characteristic absorption bands, which were observed as follows (Figure 2A): PU IR ν_{\max} (cm^{-1}): 3319 (N–H stretch), 2854–2918 (C–H stretch), 1688 (C=O stretch). PCDA IR ν_{\max} (cm^{-1}): 2847–2921 (C–H stretch), 1693 (C=O stretch), 1466 (C–H bend). PCDA-NHS IR ν_{\max} (cm^{-1}): 2922–2851 (C–H stretch), 1818 (C=O stretch, NHS ester), 1787 (symmetric C=O stretch, NHS imidyl C=O), 1742 (asymmetric C=O stretch, NHS imidyl C=O), 1466 (C–H bend). Notably, the carbonyl C=O stretching band shifted from 1693 cm^{-1} in unmodified PCDA to 1818 cm^{-1} in PCDA-NHS, with NHS imidyl C=O stretching bands observable at 1787 cm^{-1} (symmetric) and 1742 cm^{-1} (antisymmetric), confirming successful formation of the ester resulting from NHS modification (Figure 2A). After electrospinning, the membranes containing NHS-activated monomers were analyzed with ATR-FTIR to confirm that the activated monomers remained conjugated with NHS and survived the electrospinning process (Figure 2B). The characteristic peaks

associated with the NHS-activated monomer at 1815 and 1780 cm^{-1} were observed in the ATR-FTIR spectrum of the membranes post-electrospinning, which confirms that the NHS-ester was preserved throughout the electrospinning process. By subtracting PU from the ATR-FTIR spectrum of the “P-NHS” membrane, the NHS-ester peaks can clearly be observed: the carbonyl C=O stretch due to NHS ester formation was observed with the expected shift to 1815 cm^{-1} (compared to 1690 cm^{-1} in unmodified PCDA), with NHS imidyl C=O stretch at 1780 and 1739 cm^{-1} , which confirms that the NHS-ester was preserved throughout the electrospinning process. Furthermore, an additional carbonyl peak appeared at 1689 cm^{-1} in the spectra of the P-NHS nanofibers, located at lower wavenumber due to hydrogen bonding between unmodified PCDA monomers. The incorporation of unmodified PCDA in the 5:1 PCDA:PCDA-NHS blend was necessary to encourage self-alignment of the monomers during the electrospinning process via hydrogen bonding between the carboxylic acid groups in the unmodified monomers. Polymerization of diacetylene monomers requires topochemical reaction conditions in which the monomers should be separated by a distance of ≤ 3.8 Å with a translational repeat spacing of ≤ 4.9 Å as well as have a 45° orientation to the crystal axis in

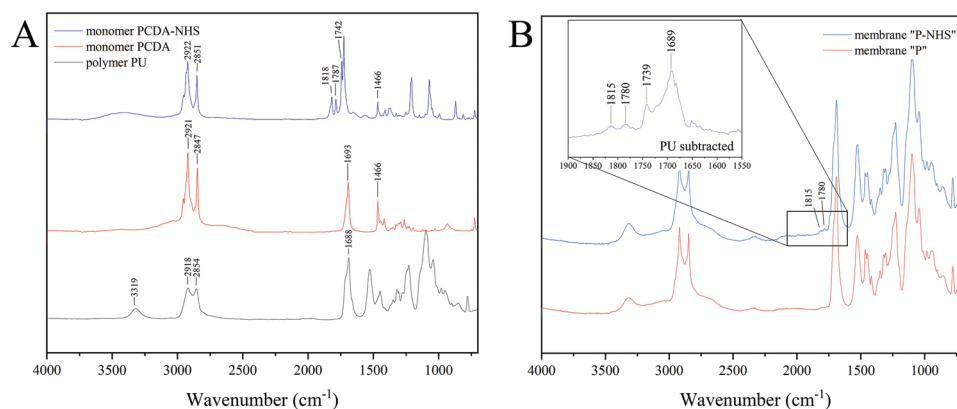


Figure 2. ATR-FTIR spectra of A) PU, PCDA, and PCDA-NHS prior to electrospinning, and B) electrospun diacetylene membranes. P and P-NHS.

Table 1. Efficiency of aptamer conjugation to electrospun polydiacetylene membranes.

Sample	Conjugation Efficiency (%)		Aptamer Conjugation [nmol g ⁻¹]	
	0.1 μ M	0.5 μ M	0.1 μ M	0.5 μ M
P-F ₂₃	0.046 \pm 0.001	0.187 \pm 0.009	41 \pm 1	165 \pm 8
P-St21Lp17	0.045 \pm 0.009	0.220 \pm 0.004	39 \pm 8	195 \pm 3
T-F ₂₃	0.033 \pm 0.003	0.180 \pm 0.005	31 \pm 3	169 \pm 5
T-St21Lp17	0.041 \pm 0.003	0.238 \pm 0.001	38 \pm 3	223 \pm 1

order for the 1,4-addition reaction to occur.^[38] In our preliminary experiments using PCDA-NHS alone for the nanofiber diacetylene compositor, UV-polymerization of the nanofibers post-electrospinning was unsuccessful since the self-alignment of the monomers during electrospinning was insufficient due to reduced hydrogen bonding in the NHS-modified monomers. By reducing the PCDA-NHS content to a 5:1 PCDA:PCDA-NHS ratio, the monomer alignment was sufficient for successful UV-photopolymerization which resulted in a color change from white to deep blue.

To achieve targeted detection of *P. aeruginosa*, the polydiacetylene nanofibers were modified with two aptamers, namely F₂₃ and St21Lp17, which were chosen for this proof-of-concept study based on their high binding affinity for *P. aeruginosa*.^[33,34] The amine-terminated aptamers F₂₃ and St21Lp17 were conjugated to the NHS-activated diacetylene monomers post-electrospinning by immersing the membranes in a solution containing the aptamers at 0.1 or 0.5 μ M concentration. The aptamer conjugation efficiency was dependent on the concentration of aptamer in the reaction liquor, with better efficiency at 0.5 μ M compared to 0.1 μ M. The loadings achieved at 0.5 μ M aptamer concentration range from 165–223 nmol g⁻¹, whereas loadings at 0.1 μ M were notably lower, ranging from 31–41 nmol g⁻¹ (Table 1). Overall, the conjugation of the aptamer St21Lp17 yielded higher concentrations of aptamer on the membranes compared to aptamer F₂₃. At a 0.5 μ M aptamer liquor concentration, the quantity of grafted aptamer St21Lp17 exceeded the amount of grafted F₂₃ by 18% for P membranes and 32% for T membranes. This boosted grafting efficiency for the St21Lp17 aptamer can be attributed to the structural differences between the aptamers. The aptamer St21Lp17 has a shorter overall strand length compared to aptamer F₂₃, with 38 bases for St21Lp17 compared to 60 for F₂₃. The longer strand length of F₂₃ bears a larger number of negatively charged phosphate groups in the single-stranded DNA backbone, which could result in negative-charge repulsion and limit the grafting efficiency. Other authors have similarly noted the limited surface-grafting efficiency of DNA due to negative charge repulsion effects.^[39] Steric hindrance due to the larger size of F₂₃ compared to St21Lp17 could also play a role in limiting the modification efficiency. F₂₃ also has a bulkier overall structure featuring a large central loop with one branching stem-loop,^[33] whereas St21Lp17 has a single stem-loop structure.^[34] Overall, the efficiency of conjugation was low compared to the available number of sites for reaction with the amine-terminated aptamers based on the loaded amount of PCDA-NHS or TCDA-NHS: in all cases, the conjugation efficiency was <0.24%. Aside from the previously mentioned factors such as repulsion between the negatively charged aptamers during grafting and steric hindrance due

to the bulky secondary structure of the aptamers, the major factor limiting the conjugation efficiency is likely the hydrophobicity of the PU fiber surface. Additionally, blend electrospinning carries the obvious limitation that only the accessible PCDA-NHS or TCDA-NHS groups at the fiber surface are available for surface modification, whereas the majority of the loaded PCDA-NHS and TCDA-NHS remain trapped within the fiber bulk material.

The aptamer-conjugated membranes were UV polymerized with 40 000 μ J cm⁻² of 254 nm UV light per side (after aptamer conjugation), which was sufficient to induce a color change from white (unpolymerized) to deep blue (polymerized). The polymerized membranes showed a characteristic reflectance minimum at 640 nm with high reflectance in the blue visible light region (<450 nm). The characteristic visible light reflectance of the blue-phase polydiacetylene membranes was unchanged after the conjugation of aptamers St21Lp17 and F23 (Figure 3). It is well known that UV exposure can induce the formation of photodimers in DNA sequences which alter their structure. Although UV polymerization prior to aptamer conjugation may be

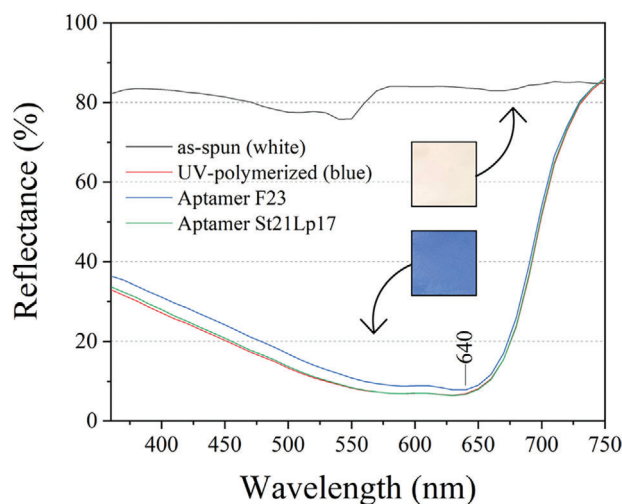


Figure 3. UV-vis reflectance spectra of 3:1 PU:PCDA membranes before and after conjugation of aptamers F₂₃ and St21Lp17. “As-spun”: the reflectance of membrane P (3:1 PU:PCDA) prior immediately after electrospinning, prior to UV polymerization. “UV-polymerized”: reflectance of membrane P (3:1 PU:PCDA) after polymerization with UV light (40 000 μ J cm⁻² UV light per side, 254 nm). “Aptamer F-23”: reflectance of the P-NHS membrane after conjugation of aptamer F-23 and UV-polymerization (40 000 μ J cm⁻² UV light per side, 254 nm). “Aptamer St21Lp17”: reflectance of the P-NHS membrane after conjugation of aptamer St21Lp17 and UV-polymerization (40 000 μ J cm⁻² UV light per side, 254 nm).
















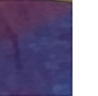
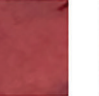



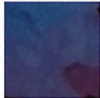

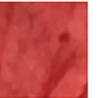

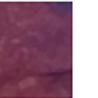




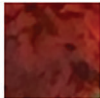



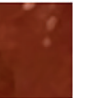

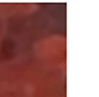


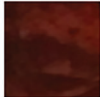



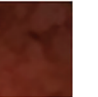

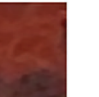
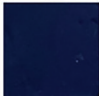

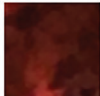






Strain		27853	PA01172	PA01	PA0386	PA0200	PA0238	73104	PA0325
Conc.	Initial	1.5 ± 0.5	3.9 ± 0.7	1.6 ± 0.3	9.8 ± 0.9	1.7 ± 0.8	3.6 ± 0.8	1.1 ± 0.2	5.5 ± 0.9
(CFU/cm ²)	(t=0)	$\times 10^9$	$\times 10^9$	$\times 10^{10}$	$\times 10^9$	$\times 10^9$	$\times 10^{10}$	$\times 10^{10}$	$\times 10^9$
P									
P-F ₂₃									
P-St21Lp17									
T									
T-F ₂₃									
T-St21Lp17									

Figure 4. Blue to red color change in response to exposure to various strains of *P. aeruginosa* for 3 h, lawn concentration ranged from $\approx 10^9$ – 10^{10} CFU/cm² (high concentration).

desirable to prevent UV-induced damage to the structure of the DNA aptamers, our experiments showed that UV polymerization prior to aptamer conjugation was not feasible due to the blue-to-red color-changing induced by the reaction of the amine-terminated aptamers with NHS-activated diacetylene monomers. The exposure time and energy levels were deliberately kept low to minimize potential damage to the DNA aptamers' structure.

2.2. Colorimetric Response to Bacteria

The aptamer-modified polydiacetylene nanofibrous membranes were tested in direct contact with *P. aeruginosa* ATCC 27853 lawns to analyze the rate and magnitude of color changing in response to the aptamer bacterial target (Figures 4 and 5). Reflectance spectra of the membranes were measured by GretagMacbeth Color-Eye 2180UV before and after exposure to *P. aeruginosa* to quantify the color change response of the nanofibers in direct contact with bacteria (Figure 6). The membrane containing unmodified PCDA did not exhibit a substantial change in reflectance over 5 h contact with *P. aeruginosa* ATCC 27853. In contrast, the aptamer-modified P-F₂₃ and P-St21Lp17 both exhibited a gradual increase in reflectance at 640 nm (red) and a decrease in reflectance from 360–540 nm (blue) associated with blue to red

color changing over the course of 1–5 h contact. The core mechanism of polydiacetylene color changing is well-understood and involves a conformational change to the polymer backbone triggered by the interaction of various stimuli. These interactions disrupt the conjugated backbone of the polymer, typically by causing rotation of the polymer backbone from planar to non-planar conformation. This rotation alleviates strain on the planar conjugated ene-yne backbone through segmental rearrangement.^[40,41] As the conjugated system shortens due to backbone rotation, the HOMO-LUMO bandgap widens. Consequently, the polymer absorbs light at a higher energy (shorter wavelength), leading to the observed blue-to-red color shift. Aptamer conjugation to the pendant side-chains introduces a new dimension to the color change mechanism. When aptamers bind to their target bacteria, the bulky aptamer-bacteria complex creates steric hindrance, disrupting the packing of the polydiacetylene side chains.^[42] This additional bacteria-specific disruption amplifies the backbone torsion and color change, explaining the sensitivity and specificity observed with aptamer-modified PCDA membranes.^[42]

For membranes containing the TCDA monomer, rapid non-specific color changing was achieved upon contact with the target strain, with blue-to-red color changing achieved after 2 h contact. The non-modified TCDA membranes responded to the target strain of *P. aeruginosa* without aptamer modification. TCDA












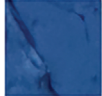

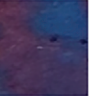











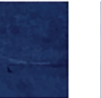



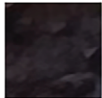

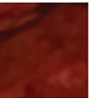

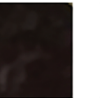


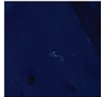




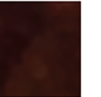
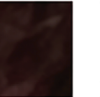

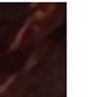
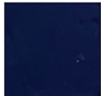
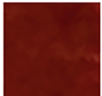
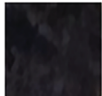


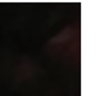
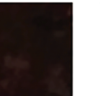

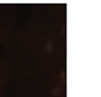
Strain		27853	PA01172	PA01	PA0386	PA0200	PA0238	73104	PA0325
Conc.	Initial	7.9 ± 0.8	1.0 ± 0.1	5.0 ± 0.3	7.3 ± 0.5	1.7 ± 0.4	2.8 ± 0.8	2.5 ± 0.8	1.1 ± 0.1
(CFU/cm ²)	(t=0)	$\times 10^7$	$\times 10^7$	$\times 10^8$	$\times 10^7$	$\times 10^7$	$\times 10^7$	$\times 10^7$	$\times 10^8$
P									
P-F ₂₃									
P-St21Lp17									
T									
T-F ₂₃									
T-St21Lp17									

Figure 5. Blue to red color change in response to exposure to various strains of *P. aeruginosa* for 3 h, lawn concentration ranged from $\approx 10^7$ – 10^8 CFU/cm² (low concentration).

has a shorter side chain length relative to PCDA, which reduces the strength of dispersion interactions between the tails. As a result, the energy barrier to induce backbone torsion and the ensuing blue to red color change is lower for TCDA-based polydiacetylenes. For the case of the TCDA-based membranes, aptamer conjugation did not result in an improved sensitivity of color changing.

Colorimetric response (CR%) was calculated to represent the extent of blue to red color changing (Figure 7).^[18,35] CR% was calculated as follows: $CR\% = [(PB_0 - PB)/PB_0] \times 100$ where PB_0 is the initial “percent blue” and PB is the “percent blue” after exposure to the stimulus: $PB = A_{640\text{ nm}} / (A_{540\text{ nm}} + A_{640\text{ nm}})$. The colorimetric response was greatest for the non-aptamer modified TCDA membranes— $11.6 \pm 0.2\%$ after 2 h, reaching $16.5 \pm 0.2\%$ after 5 h. Interestingly, the magnitude of color changing for the aptamer modified TCDA membranes T-F₂₃ and T-St21Lp17 was lower relative to unmodified TCDA (CR% of $7.5 \pm 0.5\%$ and $7.1 \pm 0.8\%$ respectively). The reduced sensitivity after aptamer conjugation may indicate that the steric bulk added by aptamer conjugation reduces the mobility of the polydiacetylene, which would outweigh the inherent benefit of using the shorter chain length monomer to reduce the dispersion forces between the side-chains and hence create better mobility of the polymer backbone to create the torsion responsible for the blue-to-

red color change. The colorimetric response of the PCDA-based membranes highlighted the benefit of aptamer conjugation for improving the sensitivity of color changing in a specific manner. The PCDA membrane alone displayed negligible color change over the course of the 5 h contact period, with a net CR% of $0.3 \pm 0.2\%$ after 5 h. The conjugation of the aptamer F₂₃ or St21Lp17 was highly effective to boost the CR%, and the membranes P-F₂₃ and P-St21Lp17 achieved a CR% of $5.44 \pm 0.04\%$ and $4.41 \pm 0.08\%$ respectively after 5 h. Both of the aptamers used in the study had a K_d reported in the low nM range ($K_d = 17.27 \pm 5.00$ nM for F₂₃ and 13.5 ± 2 nM St21Lp17 respectively).^[33,34] Despite aptamer St21Lp17 having a higher reported binding affinity (lower K_d) and higher grafted efficiency of 195 ± 3 nmol g^{−1} compared to 165 ± 8 nmol g^{−1} for aptamer F₂₃, the aptamer St21Lp17 did not exhibit a boosted CR% relative to P-F₂₃.

The limit of detection (LOD) toward a model strain of *P. aeruginosa* (ATCC 27853) was calculated as follows: $LOD = y_{\text{blank}} + 3 SD_{\text{blank}}$ where y_{blank} is the average signal intensity (CR%) of the blank control and SD_{blank} is the standard deviation of the blank control (Figure S3, Supporting Information). The LOD for the aptamer modified membranes P-F₂₃ and P-St21Lp17 were 1.42×10^6 CFU/cm² and 4.46×10^6 CFU/cm², respectively. The LOD for unmodified membrane “P” was not quantified since the colorimetric response of the membranes did not exceed the

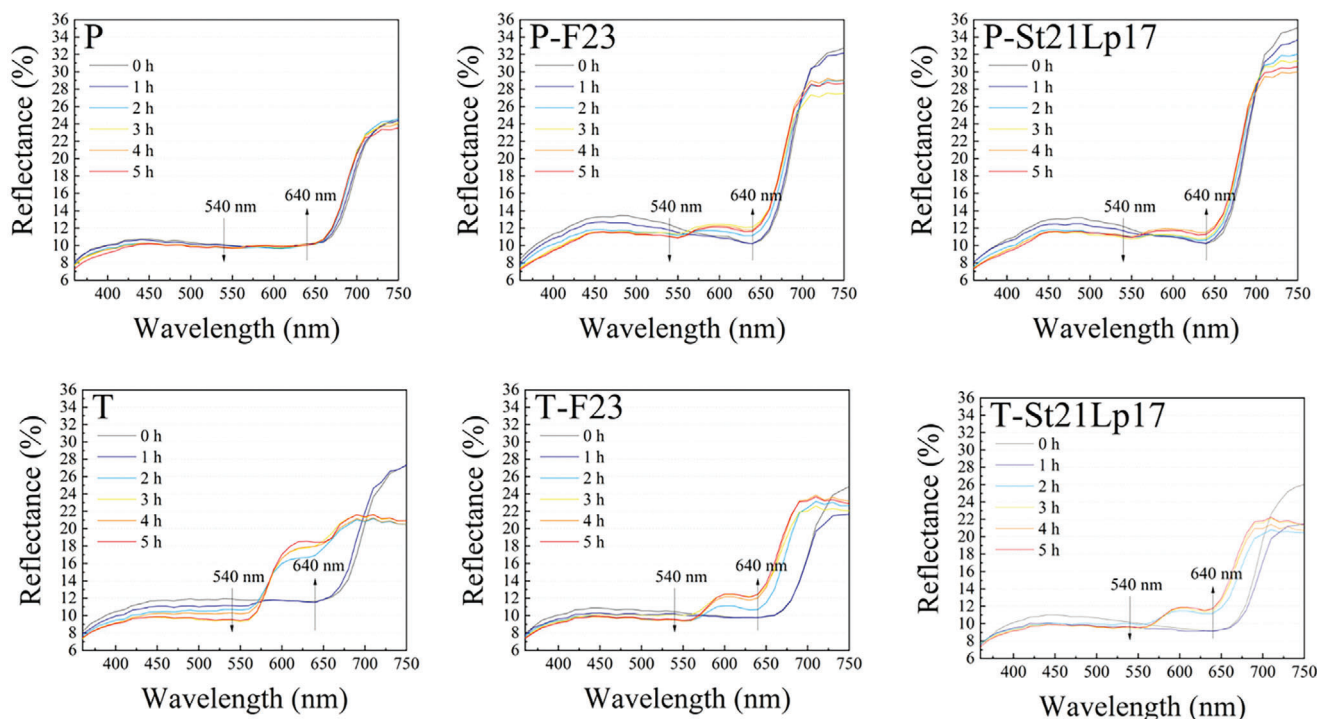


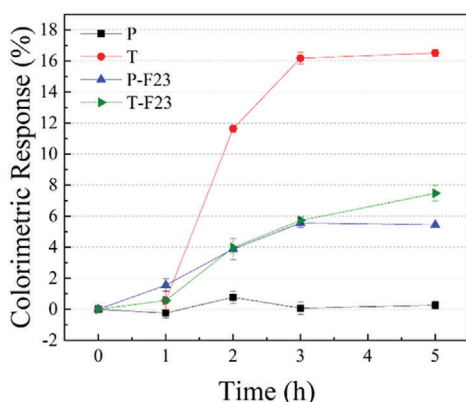
Figure 6. Reflectance spectra of aptamer-conjugated membranes throughout 0–5 h of direct-contact with a *P. aeruginosa* lawn (ATCC 27 853) at concentration of $4.8 \pm 2.1 \times 10^7$ CFU/cm² (target strain).

threshold defining the LOD at $y_{\text{blank}} + 3 \text{SD}_{\text{blank}}$, since the membranes did not exhibit a color change from blue to red at the highest tested concentration of 2.14×10^8 CFU/cm² after 3 h contact. This demonstrates the clear benefit of aptamer conjugation to improve the LOD toward the target bacteria. By replacing PCDA with the shorter chain-length monomer TCDA, lower LODs were achieved at values of 4.7×10^5 , 5.9×10^5 , and 2.9×10^5 CFU/cm². The LOD of the membranes approaches the approximate concentration which is generally considered as the threshold for colonization to infection at $5 \times 10^4 - 4.6 \times 10^5$ CFU/cm².^[20–22] Aptamer conjugation to the TCDA-based mem-

branes did not significantly lower the LOD to the model strain of *P. aeruginosa* compared to the membrane without aptamer modification. Ultimately, this method is promising for the detection of *Pseudomonas* in the early stages of infection—further work may focus on refining the specificity of the nanofibers at the already-achieved detection levels at low bacteria concentrations.

Aptamer-conjugated membranes were tested in response to a variety of strains of *P. aeruginosa* (ATCC 27853, PA01, PA0200, PA0238, PA0325, PA0386, PA01172, and 73104) to determine the specificity of the color-change response (Figure 4; Figure S4, Supporting Information). The aptamer-modified PCDA-based

Aptamer F23



Aptamer St21Lp17

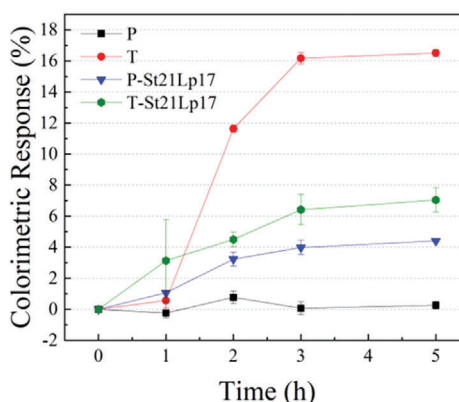


Figure 7. Colorimetric response of aptamer-conjugated membranes throughout 0–5 h of direct-contact with a *P. aeruginosa* lawn (ATCC 27853) at concentration of $4.8 \pm 2.1 \times 10^7$ CFU/cm² (target strain).

membranes (P-F₂₃ and P-St21Lp17) showed a vivid blue to red or purple color change after 3 h contact with each of the eight tested *P. aeruginosa* strains, compared to the unmodified PCDA membrane “P”, which remained blue after 3 h contact at lawn concentrations ranging from 10^9 – 10^{10} CFU/cm². This result confirms that aptamer conjugation boosts the sensitivity of polydiacetylene nanofibers for detecting the target bacterium, *P. aeruginosa*. At lower lawn concentrations of 10^7 – 10^8 CFU/cm², differences in detection sensitivity at the strain-level became evident (Figure 5). The aptamer-conjugated membranes P-F₂₃ and P-St21Lp17 exhibited a clear blue-to-pink color transition after 3 h contact with ATCC 27853, whereas the membranes remained blue in the presence of the other tested strains of *P. aeruginosa*. The enhanced affinity of the aptamer-modified membranes ATCC 27853 compared to the other tested strains of *P. aeruginosa* may arise from differential expression of surface-associated aptamer binding targets between the different bacterial strains. Aptamers can bind various bacterial targets such as lipopolysaccharides, outer membrane proteins, toxins and spores.^[43] For example, two of the tested strains in this study, *P. aeruginosa* ATCC 27853 and PAO1, display different expression levels of genes associated with the production of surface-associated proteins and lipopolysaccharides.^[44] These differences may serve as potential ligands for aptamer binding. Compared to PAO1, *P. aeruginosa* ATCC 27853 lacks the *wbp* genes encoding B-band lipopolysaccharide O antigen (except wbpX). Relative to PAO1, *P. aeruginosa* ATCC 27853 also displays higher relative expression levels of 137 genes including classes related to formation of biofilms (exopolysaccharide production, type IV pili biogenesis gene cluster, twitching motility proteins, surface adhesion (*cupA1-A4*), as well as type I, III and VI secretion systems) such as *pilQPONM*, *pilGHIJK-chpABCDE*, *pilABCDE*, *pilTU*, *pilSR-yfiT-fimTU-pilVWXYZ1Y2E*, *cupA1-A4*.^[44] However, the aptamer binding targets of aptamers F₂₃ and St21Lp17 have not been identified in prior work (by nature of the SELEX procedure for aptamer selection, prior identification of the binding ligand is not required to obtain high affinity to the target). Therefore, we cannot speculate regarding the reason for the boosted sensitivity toward the ATCC 27853 *P. aeruginosa* strain which was observed here.

In pursuit of detection sensitivity to lower bacterial concentrations, the PCDA diacetylene monomer (12 carbon alkyl tail) was replaced with a shorter chain-length monomer, TCDA (10 carbon alkyl tail) for the formation of polydiacetylene in the nanofibers. In contrast to the PCDA-based membranes, which showed improved sensitivity of *P. aeruginosa* detection after aptamer modification, the TCDA-based membranes were highly responsive toward all of the tested *P. aeruginosa* strains without aptamer modification. The unmodified “T” membranes exhibited a blue-to-red color transition toward each of the tested strains at concentrations of 10^7 – 10^8 CFU/cm². Despite having reduced sensitivity compared to the TCDA-based membranes, the stabilization effect arising from the longer side-chain of PCDA creates the benefit of improved specificity through the controlled selection of aptamers to boost the sensitivity of the PCDA-based nanofibers toward a desired bacteria species.

The membranes were also tested in direct contact with non-target bacteria species (MRSA, *S. aureus* and *E. coli*) to evaluate the specificity of the conjugated aptamers to their targeted species, *P. aeruginosa* (Figure 8 and S5, Supporting Informa-

tion). The PCDA-based membranes remained in the blue phase when contacting the non-target bacteria species throughout 3 h of direct contact at lawn concentrations ranging from 10^7 – 10^{10} CFU/cm², with the exception of *E. coli* ATCC 25922 and K88 which exhibited a purple color after 3 h contact. As expected, the TCDA-based membranes continued to show high sensitivity and non-specific color changing and exhibited a red color in response to all of the tested strains after 3 h contact. It is worth noting that the PCDA-based membranes did eventually exhibit blue-to-red color changes in response to the non-target species after extended incubation times greater than or equal to 4 h. When the incubation time was extended to 4–5 h, the following non-target species triggered a color change for the PCDA-based membranes: CA MRSA 96606, *S. aureus* ATCC 25923, *S. aureus* ATCC 29213, *E. coli* 25922, and *E. coli* K88. However, such high concentrations of non-target bacteria are irrelevant in the end-use scenario as a biosensor for in situ detection of wound infections, since such high bacteria concentrations would illicit clinical symptoms which negate the need for color change to identify the presence of infection. Interestingly, the PCDA membranes P, P-F₂₃ and P-St21Lp17 did not exhibit any color change in response to *E. coli* Top 10 ($1.8 \pm 0.3 \times 10^8$ CFU/cm²) and MRSA 33 592 ($5.9 \pm 0.2 \times 10^{10}$ CFU/cm²), even after a prolonged period of 5 h of direct contact.

In summary, the results suggest that aptamer modification is a promising strategy to achieve improved specificity of colorimetric detection of bacteria at the strain-level, as well as to boost the color-changing sensitivity of polydiacetylenes. Furthermore, the side-chain architecture of the polydiacetylene can be engineered to achieve boosted sensitivity or improve the polydiacetylene stability to prevent color changing to off-target strains of bacteria, depending on the desired behavior of the sensor. The targeted nature of the aptamer-modified membranes serves as a proof-of-concept for achieving color-based detection of a desired bacterial target, which could be generalized to other wound pathogens. The resulting aptamer/polydiacetylene nanofiber system is promising for application as a biosensor for wound infections.

3. Conclusion

In conclusion, the strategy of aptamer-modification of polydiacetylene electrospun nanofibers has shown promise for targeted color-based detection of bacteria at the species level. Two aptamers, F₂₃ and St21Lp17, were conjugated to the diacetylenes in a post-electrospinning modification step using NHS/EDC chemistry. Aptamer conjugation to the PCDA-based membranes improved the sensitivity of blue-to-red color change toward eight tested strains of *P. aeruginosa*, compared to the unmodified membranes. Furthermore, the aptamer-modified PCDA membranes responded strongly to low concentrations of the target strain *P. aeruginosa*, ATCC 27853 ($7.9 \pm 0.8 \times 10^7$ CFU/cm²) after 3 h contact, but did not exhibit a full color change within 3 h of direct contact with non-target bacteria lawns of seven tested strains of MRSA, *S. aureus* and *E. coli*. Membranes which incorporated a shorter side-chain length monomer TCDA had a CR% which was more than 2x higher compared to the aptamer-modified PCDA membranes. However, the boosted sensitivity of the TCDA-based membranes came with the drawback of reduced specificity, as








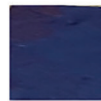
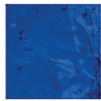




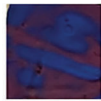

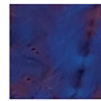


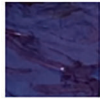


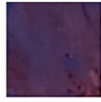

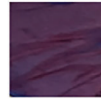

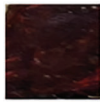



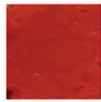
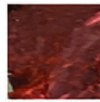
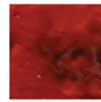

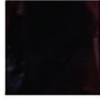
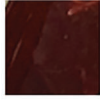
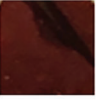
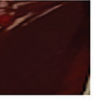

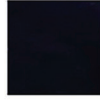
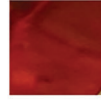
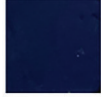
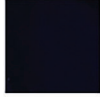
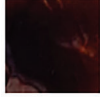
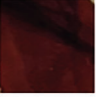

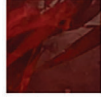
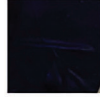
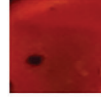
		MRSA		<i>S. aureus</i>		<i>E. coli</i>		
		ATCC	CA	ATCC	ATCC	ATCC	<i>E. coli</i>	<i>E. coli</i>
		MRSA	MRSA	SA	SA	<i>E. coli</i>	<i>E. coli</i>	<i>E. coli</i>
		33592	96606	25923	29213	25922	Top 10	K88
Strain								
Conc.	Initial	5.9 ± 0.2	6.6 ± 1.8	1.0 ± 0.9	1.1 ± 0.1	5.9 ± 2.1	4.4 ± 0.6	2.4 ± 0.6
(CFU/cm ²)	(t=0)	x 10 ¹⁰	x 10 ¹⁰	x 10 ⁸	x 10 ¹⁰	x 10 ⁷	x 10 ⁸	x 10 ⁹
P								
P-F ₂₃								
P-St21Lp17								
T								
T-F ₂₃								
T-St21Lp17								

Figure 8. Blue to red color change in response to exposure to non-target bacteria species (MRSA, *S. aureus*, and *E. coli*) for 3 h contact time.

aptamer modification did not improve the specificity of color changing for TCDA-based membranes. Our findings demonstrate that aptamer-modified polydiacetylene nanofibers offer a promising and versatile platform for developing highly specific bacterial biosensors. The inherent selectivity of aptamers allows for the creation of sensors tailored to target a wide range of bacterial strains relevant to various fields. This approach has the potential to revolutionize in situ bacterial detection in diverse applications, including clinical medicine and healthcare (e.g., rapid diagnosis of infections), food safety and quality control (e.g., identifying foodborne pathogens), environmental monitoring (e.g., detecting waterborne bacteria), water management (e.g., monitoring drinking water quality), and biosecurity (e.g., early detection of biothreat agents).

4. Experimental Section

Materials: 10,12-pentacosadiynoic acid (PCDA, ≥97.0%), 10,12-tricosadiynoic acid (TCDA, ≥98.0%), *N,N*-dimethylformamide (DMF, ≥99.8%), tetrahydrofuran (THF, ≥99.9%), ethanol (EtOH, ≥95.0%), chloroform (≥99.8%), methylene chloride (DCM, ≥99.5%),

N-hydroxysuccinimide (NHS), and 1-ethyl-3-(3-dimethylaminopropyl)carbodiimide hydrochloride (EDC) were purchased from Sigma Aldrich (St. Louis, MO, USA). Tecophilic HP-60D-35 (hydrophilic aliphatic polyurethane, PU) was purchased from Lubrizol Advanced Materials (Cleveland, OH, USA). Integra Miltex Standard 4 mm biopsy punches, LB agar (Lennox), and LB broth (Lennox) were purchased from Fisher Scientific (Nepean, ON, Canada). *P. aeruginosa* aptamers F23 (5'- CCC CCG TTG CTT TCG CTT TTC CTT TCG CTT TTG TTC GTT TCG TCC CTG CTT CCT TTC TTG -3')^[33] and St21Lp17 (5'- AAG CGT CCG TGT TCT ATC GGT AGT TGA CAC CGA CGC CT -3')^[34] were custom synthesized by Integrated DNA Technologies (IDT, Coralville, IA, USA).

Synthesis of NHS Activated PCDA and TCDA Monomers: PCDA and TCDA monomers were activated with NHS/EDC to form a reactive intermediate to enable crosslinking between the monomer carboxylic acid and the primary amine group of C6-amino modified aptamers. PCDA and TCDA were activated with NHS according to well-documented procedure reported elsewhere.^[29] To activate PCDA or TCDA with NHS, 1.035 g (5.41 mmol) EDC and 0.62 g (5.41 mmol) NHS were added to 1.35 g (3.6 mmol) PCDA or 1.25 g (3.6 mmol) TCDA in 10.0 mL DCM and stirred for 2.0 h in the dark. DCM was removed by vacuum. The NHS-activated products were purified by extraction with ethyl acetate and dried in vacuo. The final product, 10–12 pentacosadiynoic acid-*N*-hydroxysuccinimide (PCDA-NHS) was obtained as a white solid with yield of 78.95%. 10–12 tricosadiynoic acid-*N*-hydroxysuccinimide (TCDA-NHS)

Table 2. Electrospinning parameters for membrane fabrication.

Sample	Diacytlyene Ratio	Composition				
		PU [w/v %]	PCDA [w/v %]	TCDA [w/v %]	PCDA-NHS [w/v %]	TCDA-NHS [w/v %]
P	PCDA	6.0	2.0	-	-	-
T	TCDA	6.0	-	2.0	-	-
P-NHS	5:1 PCDA:PCDA-NHS	6.0	0.33	-	1.67	-
T-NHS	5:1 TCDA:TCDA-NHS	6.0	-	1.67	-	0.33

*all membranes contain diacytlyene monomers at a ratio of 3:1 PU:diacytlyene. Monomer composition varies as described.

was obtained as a white solid with yield of 92.1%. PCDA-NHS and TCDA-NHS were stored in the dark at -20°C . Structures of the NHS-activated monomers were confirmed with ^1H -nuclear magnetic resonance (^1H -NMR, Ascend 400, Bruker, Karlsruhe, Germany): ^1H -NMR of PCDA-NHS (400 MHz, CDCl_3): δ 0.891 (t, 3H), 1.214–1.461 (m, 28H), 1.523 (p, 4H), 1.751 (p, 2H), 2.251 (t, 4H), 2.609 (t, 2H), 2.847 (m, 4H) (Figure S1, Supporting Information). ^1H -NMR of TCDA-NHS (400 MHz, CDCl_3): δ 0.895 (t, 3H), 1.225–1.467 (m, 24H), 1.528 (p, 4H), 1.756 (p, 2H), 2.256 (t, 4H), 2.614 (t, 2H), 2.852 (m, 4H) (Figure S2, Supporting Information).

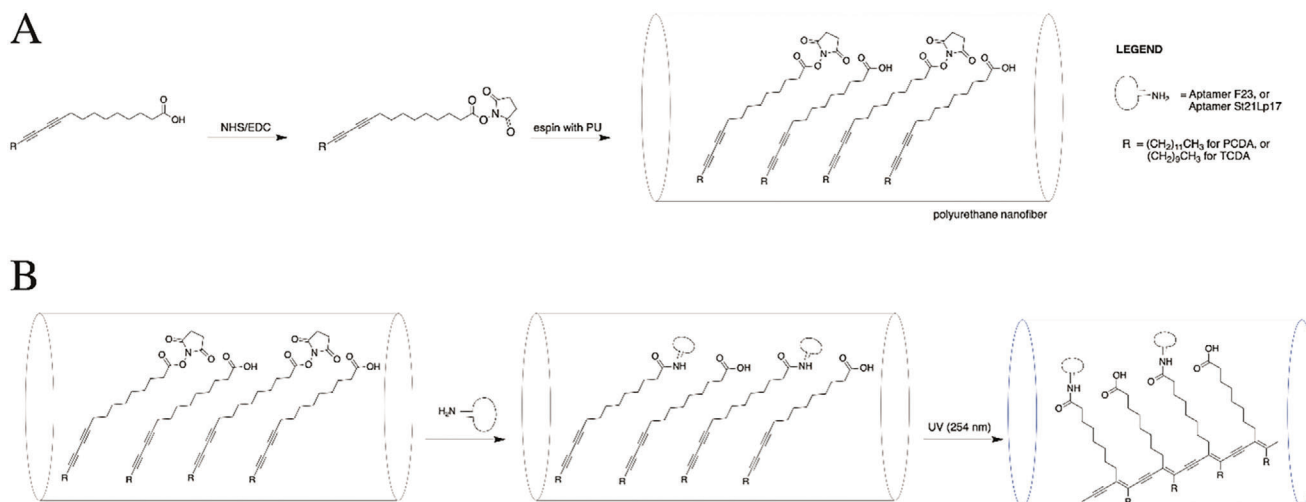
Electrospinning: PCDA or TCDA monomers were incorporated into the shell of electrospun nanofibers with medical grade PU as a matrix polymer to increase the viscosity of the solution for electrospinning. The influence of PCDA or TCDA monomer composition on the sensitivity of the membranes was explored since the monomer side-chain length has previously been reported to influence the responsiveness of polydiacytlenes.^[35] TCDA has shorter side-chain length compared to PCDA, so the dispersion forces between the TCDA side chains were lower relative to PCDA, allowing TCDA membranes to respond more easily to stimulus resulting in a lower threshold of bacteria detection. PCDA or TCDA were incorporated into nanofibers at a 3:1 ratio of polyurethane to diacytlyene (3:1 PU:PCDA (membrane “P”) or 3:1 PU:TCDA (membrane “T”).

Aptamers were conjugated to the surface of the nanofiber membranes to achieve targeted bacterial detection of *P. aeruginosa* ATCC 27853. To allow for aptamer conjugation, 3:1 PU:PCDA or 3:1 PU:TCDA membranes were electrospun with NHS-activated PCDA or TCDA monomers at ratios of 5:1 PCDA:PCDA-NHS (membrane “P-NHS”) or 5:1 TCDA:TCDA-NHS (membrane “T-NHS”). Compositional information and abbreviations for the various nanofiber formulations are summarized in Table 2.

For electrospinning, PU and diacytlyene were dissolved at the desired ratio in 1:1 DMF:THF. The solutions were stirred overnight at room tem-

perature to ensure homogeneity. The composition of the solutions for electrospinning is described in Table 2. Solutions were sonicated immediately prior to electrospinning to improve homogeneity. Solutions were electrospun with a flow rate of 1.4 mL h^{-1} , voltage of 24.1 kV and needle-collector distance of 22.8 cm onto an aluminum foil-covered collector using an NE300 electrospinner (Inovenso, Turkey) at a temperature of 21°C and RH of 25%. The unpolymerized membranes were stored in the dark to protect the light-sensitive monomers.

Aptamer Conjugation to NHS-Activated Polydiacytlyene Membranes: Two aptamers were chosen for conjugation to the NHS-activated polydiacytlyene membranes – aptamer F_{23} (identified by Wang et al. via whole-cell SELEX toward *P. aeruginosa* ATCC 27853^[33]) and aptamer St21Lp17 (identified by Soundy and Day via whole-cell SELEX toward *P. aeruginosa* PA692 biofilm^[34]). The aptamers differ in structure and binding affinity for *P. aeruginosa*. Aptamer F_{23} features a large central loop with a single branching stem-loop and K_d of $17.27 \pm 5.00\text{ nM}$, and aptamer St21Lp17 has a single stem-loop with K_d of $13.5 \pm 2\text{ nM}$. The aptamers were chosen for this study based on high binding affinity for the targeted bacteria, *P. aeruginosa* (both aptamers had K_d in the low nanomolar range). Prior to UV-polymerization, the as-spun membranes were immersed in 0.5 or $0.1\text{ }\mu\text{M}$ solution of aptamer F_{23} or St21Lp17 at a liquor ratio of 2 mg mL^{-1} (membrane mass per buffer volume) in 0.01 M PBS, pH 7.0, and incubated for 24 h with shaking at room temperature followed by rinsing with DI water. The aptamers F_{23} and St21Lp17 were conjugated to the membrane based on NHS/EDC chemistry, where the amine-terminated aptamers reacted with NHS-activated PCDA and TCDA monomers to form an amide bond (Scheme 1). Unreacted NHS-esters were quenched using 18.3 mM ethanolamine in 0.01 M PBS, pH 7.0 for 1 h at room temperature followed by rinsing with DI water. The membranes were dried in the dark before UV-polymerization with $40\text{ }000\text{ }\mu\text{J cm}^{-2}$ UV light per side (254 nm).



Scheme 1. Conjugation of aptamers F_{23} and St21Lp17 to NHS-activated 3:1 PU:PCDA or 3:1 PU:TCDA membranes.

UV-polymerization resulted in a color change from the white as-spun membrane to dark blue. The absorbance of the supernatant aptamer solution was analyzed by a microplate reader at 260 nm to determine the aptamer conjugation efficiency.

Nanofiber Characterization: Nanofiber morphology was characterized using SEM (FEI Nano Nova). Samples were sputter coated for 45 s with gold-palladium (60:40) prior to imaging. SEM was conducted with an accelerating voltage of 10.0 kV and fiber diameters were measured using ImageJ. Chemical structure of the membranes was confirmed by ATR-FTIR (Thermo Scientific, Nicolet iS10) and $^1\text{H-NMR}$ (Ascend 400, Bruker, Karlsruhe, Germany).

Bacterial Culture: To confirm the specificity of the color-changing response to the targeted bacteria (*P. aeruginosa*), the aptamer-conjugated membranes were tested in response to various strains of *P. aeruginosa* ATCC 27853, PA01, PA0200, PA0238, PA0325, PA0386, PA01172, and clinical isolate 73104 (description of strains provided in Table S1, Supporting Information 44–49), as well as non-target bacteria species *E. coli* (ATCC 25922, Top 10, K88) *S. aureus* (ATCC 25923, ATCC 29213) and MRSA (ATCC 33592, CA 96606). The various bacteria strains of *P. aeruginosa*, *E. coli*, *S. aureus* or MRSA were streaked on LB agar and incubated for 18 h at 37 °C. For the preparation of overnight broth culture, *P. aeruginosa*, *E. coli*, *S. aureus* or MRSA colonies were suspended in 0.01 M PBS to a turbidity of 0.5 (MacFarland standard) and diluted by a factor of 100X in 0.01 M PBS, followed by adding 15.0 μL of the diluted suspension to 45.0 mL LB broth in a 50 mL tube. The broth culture was incubated for 18 h at 37 °C with shaking at 140 rpm.

Colorimetric Response to Bacteria: To prepare bacterial lawns, overnight suspensions prepared as previously described were adjusted to a turbidity of 0.5 (MacFarland standard), diluted by a factor of 100X, and spread on LB agar (100 μL) followed by incubation at 37 °C for various time intervals (5–10 h) to produce bacterial lawns in a range of concentrations. After the incubation, 1 cm x 1 cm membrane samples were placed directly onto the lawns and monitored by naked eye for a color change for 3 h at 37 °C.

The reflectance spectra of the membranes were measured by spectrophotometer (GretagMacbeth ColorEye 2180UV) with CIE Illuminant D65 and 10° observer with the membranes in situ in the Petri dish. Photos and spectrophotometer readings were taken hourly from 0–5 h, and the bacterial lawn concentration in CFU/cm² was quantified at the initial time period. Colorimetric response (% CR) was calculated as follows: % CR = $[(\text{PB}_0 - \text{PB}) / \text{PB}_0] \times 100$, where PB is “percent blue”: $\text{PB} = A_{\text{blue}} / (A_{\text{red}} + A_{\text{blue}})$. A_{blue} is the absorbance at 640 nm and A_{red} is the absorbance at 540 nm.

To quantify the lawn concentration, cylindrical agar plugs were removed from the lawns with a 4 mm Integra Miltex Standard Biopsy Punch and vortexed for 2 min in 1.0 mL PBS to detach the bacteria from the surface of the agar. The concentrations of the bacterial suspensions were quantified according to drop-plating procedure. Briefly, the suspensions were subjected to serial 10-fold dilutions in PBS followed by plating 30.0 μL drops of each dilution respectively, onto LB agar. Colonies were counted following incubation at 37 °C for 18 h.

Statistical Analysis: Data are presented as mean \pm standard deviation (SD). The number of replicates is indicated as the *n*-value. Fiber diameter data were analyzed by one-way ANOVA with Tukey's correction ($p < 0.05$). All statistical analyses were conducted using SAS software (Version 9.4, SAS Institute, Cary NC).

Supporting Information

Supporting Information is available from the Wiley Online Library or from the author.

Acknowledgements

The authors gratefully acknowledge the financial support from the Research Manitoba Mid-Career Operating Grant, the Natural Sciences

and Engineering Research Council of Canada (NSERC) Discovery Grant (RGPIN-2019-06094), Cystic Fibrosis Foundation, and the Canada Foundation for Innovation (#23679).

Conflict of Interest

The authors declare no conflict of interest.

Data Availability Statement

The data that support the findings of this study are available from the corresponding author upon reasonable request.

Keywords

aptamers, electrospinning, point-of-care testing, polydiacetylenes, wound infection

Received: February 26, 2024

Revised: May 9, 2024

Published online:

- [1] H. K. Estahbanati, P. P. Kashani, F. Ghanaatpisheh, *Burns* **2002**, *28*, 340.
- [2] R. Serra, R. Grande, L. Butrico, A. Rossi, U. F. Settimio, B. Caroleo, B. Amato, L. Gallelli, S. De Franciscis, *Expert Rev. Anti. Infect. Ther.* **2015**, *13*, 605.
- [3] H. Barbara, P. Iglewski, in *Medical Microbiology*, (Ed. S. Baron), 4th ed., University of Texas Medical Branch at Galveston, Galveston, TX **1996**.
- [4] D. Church, S. Elsayed, O. Reid, B. Winston, R. Lindsay, *Clin. Microbiol. Rev.* **2006**, *19*, 403.
- [5] E. E. Tredget, H. A. Shankowsky, A. M. Joffe, T. I. Inkson, K. Volpel, W. Paranchych, P. C. Kibsey, J. D. MacGregor Alton, J. F. Burke, *Clin. Infect. Dis.* **1992**, *15*, 941.
- [6] A. D. Armour, H. A. Shankowsky, T. Swanson, J. Lee, E. E. Tredget, *J. Trauma – Inj. Infect. Crit. Care.* **2007**, *63*, 164.
- [7] P. Pachori, R. Gothalwal, P. Gandhi, *Genes Dis* **2019**, *6*, 109.
- [8] D. Trevas, A. M. Caliendo, K. Hanson, J. Levy, C. C. Ginocchio, *Clin. Infect. Dis.* **2021**, *72*, e893.
- [9] T. R. Dargaville, B. L. Farrugia, J. A. Broadbent, S. Pace, Z. Upton, N. H. Voelcker, *Biosens. Bioelectron.* **2013**, *41*, 30.
- [10] D. Sharp, P. Gladstone, R. B. Smith, S. Forsythe, J. Davis, *Bioelectrochemistry* **2010**, *77*, 114.
- [11] Y. Sun, C. Zhao, J. Niu, J. Ren, X. Qu, *ACS Cent. Sci.* **2020**, *6*, 207.
- [12] J. Zhou, A. L. Loftus, G. Mulley, A. T. A. Jenkins, *J. Am. Chem. Soc.* **2010**, *132*, 6566.
- [13] J. Zhou, T. N. Tun, S. ha Hong, J. D. Mercer-Chalmers, M. Laabei, A. E. R. Young, A. T. A. Jenkins, *Biosens. Bioelectron.* **2011**, *30*, 67.
- [14] D. Sharp, S. Forsythe, J. Davis, *Biochem.* **2008**, *144*, 87.
- [15] A. Hasmann, U. Gewessler, E. Hulla, K. P. Schneider, B. Binder, A. Francesko, T. Tzanov, M. Schintler, J. Van der Palen, G. M. Guebitz, E. Wehrschuetz-Sigl, *Exp. Dermatol.* **2011**, *20*, 508.
- [16] V. Sridhar, K. Takahata, *Sens. Actuators, A Phys.* **2009**, *155*, 58.
- [17] J. Phair, L. Newton, C. McCormac, M. F. Cardosi, R. Leslie, J. Davis, *Analyst* **2011**, *136*, 4692.
- [18] J. P. Yapor, A. Alharby, C. Gentry-Weeks, M. M. Reynolds, A. K. M. M. Alam, Y. V. Li, *ACS Omega* **2017**, *2*, 7334.
- [19] N. T. Thet, D. R. Alves, J. E. Bean, S. Booth, J. Nzakizwanayo, A. E. R. Young, B. V. Jones, A. T. A. Jenkins, *ACS Appl. Mater. Interfaces.* **2016**, *8*, 14909.

- [20] W. Majewski, Z. Cybulski, M. Napierala, F. Pukacki, R. Staniskewski, K. Pietkiewicz, S. Zapalski, *Int. Angiol.* **1995**, *14*, 381.
- [21] D. Raahave, A. Friis-Møller, K. Bjerre-Jepsen, J. Thiis-Knudsen, L. Rasmussen, *Arch. Surg.* **1986**, *121*, 924.
- [22] P. G. Bowler, B. I. Duerden, D. G. Armstrong, *Clin. Microbiol. Rev.* **2001**, *14*, 244.
- [23] X. Chen, G. Zhou, X. Peng, J. Yoon, *Chem. Soc. Rev.* **2012**, *41*, 4610.
- [24] J. Wu, A. Zawistowski, M. Ehrmann, T. Yi, C. Schmuck, *J. Am. Chem. Soc.* **2011**, *133*, 9720.
- [25] B. W. Davis, A. J. Burris, N. Niamnont, C. D. Hare, C. Chen, M. Sukwattanasinitt, Q. Cheng, *Langmuir* **2014**, *30*, 9616.
- [26] X. Qian, B. Städler, *Chem. Mater.* **2019**, *31*, 1196.
- [27] E. Lebègue, C. Farre, C. Jose, J. Saulnier, F. Lagarde, Y. Chevalier, C. Chaix, N. Jaffrezic-Renault, *Sensors* **2018**, *18*, 599.
- [28] J. Park, S. Ku, D. Seo, K. Hur, H. Jeon, D. Shvartsman, H.-K. Seok, D. Mooney, K. Lee, *Chem. Commun.* **2016**, *52*, 10346.
- [29] Y. K. Jung, T. W. Kim, H. G. Park, H. T. Soh, *Adv. Funct. Mater.* **2010**, *20*, 3092.
- [30] M. Rangin, A. Basu, *J. Am. Chem. Soc.* **2004**, *126*, 5038.
- [31] W. Wu, J. Zhang, M. Zheng, Y. Zhong, J. Yang, Y. Zhao, W. Wu, W. Ye, J. Wen, Q. Wang, J. Lu, *PLoS One* **2012**, *7*, e48999.
- [32] A. V. Lakhin, V. Z. Tarantul, L. V. Gening, *Acta Naturae* **2013**, *5*, 34.
- [33] K. Y. Wang, Y. L. Zeng, X. Y. Yang, W. B. Li, X. P. Lan, *Eur. J. Clin. Microbiol. Infect. Dis.* **2011**, *30*, 273.
- [34] J. Soundy, D. Day, *PLoS One* **2017**, *12*, e0185385.
- [35] N. Charoenthai, T. Pattanatornchai, S. Wacharasindhu, M. Sukwattanasinitt, R. Traiphon, *J. Colloid Interface Sci.* **2011**, *360*, 565.
- [36] L. A. Mercante, A. Pavinatto, T. S. Pereira, F. L. Migliorini, D. M. dos Santos, D. S. Correa, *Sens. Actuators Rep.* **2021**, *3*, 100048.
- [37] K. Chen, W. Chou, L. Liu, Y. Cui, P. Xue, M. Jia, *Sensors* **2019**, *19*, 3676.
- [38] A. V. Hall, O. M. Musa, D. K. Hood, D. C. Apperley, D. S. Yufit, J. W. Steed, *Cryst. Growth Des.* **2021**, *21*, 2416.
- [39] W. Yang, L. Feng, *Anal. Chim. Acta.* **2024**, *1298*, 342382.
- [40] J. J. Schaefer, C. B. Fox, J. M. Harris, *J. Raman Spectrosc.* **2012**, *43*, 351.
- [41] R. W. Carpick, D. Y. Sasaki, M. S. Marcus, M. A. Eriksson, A. R. Burns, *J. Phys. Condens. Matter.* **2004**, *16*, R679.
- [42] J. T. Wen, K. Bohorquez, H. Tsutsui, *Sensors Actuators, B Chem.* **2016**, *232*, 313.
- [43] K. L. Hong, L. J. Sooter, *Biomed Res. Int.* **2015**, *2015*, 419318.
- [44] H. Cao, Y. Lai, S. Bougouffa, Z. Xu, A. Yan, *BMC Genomics* **2017**, *18*, 459.